Momentum-Resolved Two-Dimensional Spectroscopy as a Probe of Nonlinear Quantum Field Dynamics

Duilio De Santis,[1,2,*,†] Alex Gómez-Salvador,[2,*] Nataliia Bazhan,[3] Sebastian Erne,[3] Maximilian Prüfer,[3] Claudio Guarcello,[4] Davide Valenti,[1] Jörg Schmiedmayer,[3] and Eugene Demler[2]

[1]*Dipartimento di Fisica e Chimica "E. Segrè", Group of Interdisciplinary Theoretical Physics, Università degli Studi di Palermo, I-90128 Palermo, Italy*

[2]*Institute for Theoretical Physics, ETH Zurich, 8093 Zurich, Switzerland*

[3]*Vienna Center for Quantum Science and Technology (VCQ), Atominstitut, TU Wien, Vienna, Austria*

[4]*Dipartimento di Fisica "E. R. Caianiello", Università degli Studi di Salerno, I-84084 Fisciano, Salerno, Italy*

(Received 4 December 2025; revised 31 March 2026; accepted 30 April 2026; published 9 June 2026)

Emergent collective excitations constitute a hallmark of interacting quantum many-body systems, yet in solid-state platforms their study has been largely limited by the constraints of linear-response probes and by finite momentum resolution. We propose to overcome these limitations by combining the spatial resolution of ultracold atomic systems with the nonlinear probing capabilities of two-dimensional spectroscopy (2DS). As a concrete illustration, we analyze momentum-resolved 2DS of the quantum sine-Gordon model describing the low-energy dynamics of two weakly coupled one-dimensional Bose-Einstein condensates. This approach reveals distinctive many-body signatures, most notably asymmetric cross-peaks reflecting the interplay between isolated (B_2 breather) and continuum (B_1 pair) modes. The protocol further enables direct characterization of anharmonicity and disorder, establishing momentum-resolved 2DS as both a powerful diagnostic for quantum simulators and a versatile probe of correlated quantum matter.

DOI: 10.1103/tfdm-qshs

Introduction—Emergent collective excitations, whose properties differ qualitatively from those of their microscopic constituents, are ubiquitous in quantum many-body systems. Prominent examples include fractional excitations in quantum Hall and one-dimensional systems [1–5]. Quantum emulators based on ultracold atoms, superconducting qubits, and trapped ions enable controlled realizations of paradigmatic models, offering a unique opportunity to revisit long-standing questions in many-body physics with a new degree of control [6–11]. At the same time, the tunability of these platforms motivates the development of refined spectroscopic protocols for accessing collective excitations beyond the limits of standard solid-state approaches.

Traditionally, excitations have been probed using linear-response methods such as x-ray scattering [12,13], optical spectroscopy [14], and transport [15,16]. While invaluable, these techniques are often limited by finite momentum resolution. Recent advances in ultracold atomic platforms have allowed some of these linear response methods to be implemented even with momentum resolution [17–19], effectively surpassing the limitations of conventional solid-state experiments.

Recently, solid-state research has begun to incorporate higher-order spectroscopic techniques [20–24] to a broad array of systems. In particular, two-dimensional spectroscopy (2DS) has been applied to superconductors [25–30], correlated electron systems [31,32], ferroics [33–37], and topological phases [38–44], where it enables identification of interaction pathways [45–47], classification of bound states [48–50], and separation of homogeneous from inhomogeneous broadening [26,51–54]. Yet, the restricted momentum resolution in traditional solid-state platforms still limits the full power of these approaches. Here, we propose to combine the high momentum resolution of ultracold atoms with the nonlinear capabilities of 2DS, thereby establishing a new paradigm for probing collective excitations, see Fig. 1 for a schematic of the protocol. A comprehensive discussion on the 2DS technique can be found in Supplemental Material [55].

While our proposal is broadly applicable, we focus here on the sine-Gordon (SG) model, with a twofold motivation encompassing its rich theoretical structure and its experimental relevance. On the theoretical side, the SG model is an archetype of low-dimensional field theory: it is integrable and hosts soliton collective modes (kinks and breathers) in both its classical and quantum forms [60,61]. It is also dual to the massive Thirring

[*]These authors contributed equally to this work.
[†]Contact author: ddesantis@phys.ethz.ch

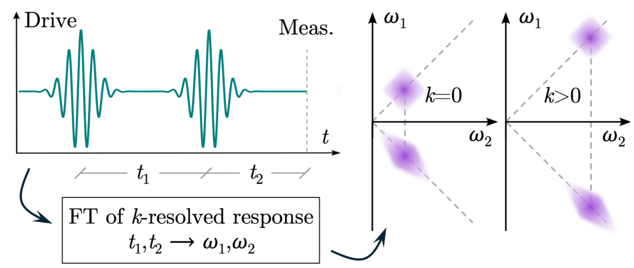

FIG. 1. Schematics of a 2DS protocol. Two perturbations, separated by a time delay $t_1 > 0$, are applied to the system. At a time $t_2 > 0$ after the second perturbation, the momentum-resolved response is measured. Fourier transforming with respect to the delays t_1 and t_2 yields a 2D map, for each value of k, in the frequency domain. The 2D map exhibits several peaks whose positions may depend on k, reflecting the momenta of the collective modes under consideration.

model [62], closely connected to Berezinskii-Kosterlitz-Thouless physics [5,63], and serves as a universal low-energy effective theory for a wide class of low-dimensional systems. On the experimental side, the SG model is realizable in ultracold atoms, where it captures the low-energy dynamics of two weakly coupled one-dimensional Bose-Einstein condensates (BECs) [64–68]. Beyond coupled BECs, the SG framework finds application in extended Josephson junctions and high-temperature superconductors [69–71], spin systems, charge-density waves, disordered systems [5,72–78], multi-component quantum Hall systems [79], domain boundaries in anisotropic magnetic systems [80], and state-of-the-art quantum processors [81].

Our objective is to demonstrate that momentum-resolved 2DS provides a powerful probe for quantum simulators. Using the SG model as a representative interacting system, we theoretically implement nonlinear response spectroscopy within a 2DS protocol. The resulting 2D maps reveal characteristic many-body features, including asymmetric cross-peak patterns arising from the coupling of isolated and continuum modes. Additionally, these protocols enable the characterization of interaction pathways, anharmonicity, and shot-to-shot disorder, which are not accessible within standard linear-response measurements.

Model and driving protocol—We write, in dimensionless units, the SG Hamiltonian as

$$H_0 = \frac{1}{2}\int dx\Big\{(\partial_x\varphi)^2 + \Pi^2 - \Delta_0\cos(\beta\varphi)\Big\}, \qquad (1)$$

where the fields φ and Π, respectively, the condensates' relative phase and density, satisfy bosonic commutation relations $[\varphi(x), \Pi(x')] = i\delta(x - x')$, and β and Δ_0 are free parameters [82]. Equation (1) is among the most universal nonlinear theories, and its exact diagonalization unveils a rich spectrum of excitations depending on the value of β: for $0 < \beta^2 < 4\pi$, both (anti)kinks and their bound states, breathers, are found; for $4\pi < \beta^2 < 8\pi$, no breather can form; finally, for $\beta^2 > 8\pi$, the cosine term becomes irrelevant in the renormalization group sense and the Luttinger liquid model is recovered [83]. The parameter β is connected to the Luttinger constant K by $\beta^2 = 2\pi/K$, and $\Delta_0 \sim J$ is the bare coupling associated with the tunneling strength J between the two condensates. Below, we focus on the regime $\beta^2 < 4\pi$ [84] for two main reasons: (i) it features the breather modes that we aim to probe to showcase the capabilities of 2DS, and (ii) it corresponds to the experimentally relevant regime for coupled condensates. A further discussion of the experimental implementation using coupled condensates, along with an estimate of the experimental parameters, is provided in the Appendix.

Our aim is to investigate the response of the SG system to a spatially homogeneous modulation of the coupling Δ_0 given by [85]

$$H_d = -\frac{1}{2}\int dx\delta\Delta_0(t)\cos(\beta\varphi), \qquad (2)$$

which corresponds, within the coupled BECs realization, to a time-dependent modulation of the tunneling strength [see Fig. 2(a)]. Note that, since both H_0 and H_d are even in the field φ, only even-power correlators can acquire an expectation value.

Henceforth, we assume a self-consistent Gaussian ansatz [56], which captures effects beyond the harmonic approximation, to characterize the dynamics of the system. This approach replaces the interacting cosine potential with an effective quadratic term whose mass is dynamically

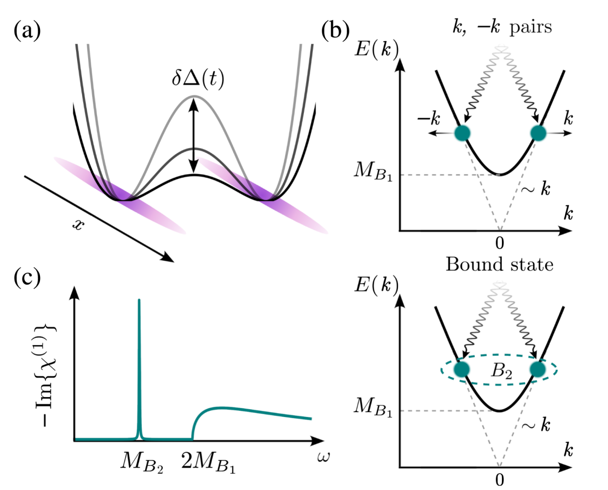

FIG. 2. (a) Pictorial representation of the external modulation of the potential barrier, see Eq. (2), in the system of two coupled condensates (in purple) in a double-well potential (gray-to-black curves). (b) Sketch of the relevant excitations accessible via tunneling modulation within our theory. (c) Imaginary part of the linear response function at total momentum $k = 0$. From left to right we distinguish two types of excitations: a sharp resonance corresponding to the $B_1 - B_1$ bound state, labeled as B_2, and a two-particle continuum composed of the $(k, -k)B_1$ pairs.

determined in a self-consistent way. In the low-T, low-β regime, the framework reliably tracks the lowest-lying SG breather excitations [55], which usually dominate the system's response [82]. More precisely, we have access to two distinct mode contributions, as schematically depicted in Fig. 2(b). The first corresponds to pairs of B_1 breathers with opposite momenta k and $-k$, which appear as a continuum in the spectral function, $-\mathrm{Im}\{\chi^{(1)}\}$, above the two-particle excitation gap $2M_{B_1}$, see Fig. 2(c). The second corresponds to the B_2 breather at zero momentum, manifesting as an isolated peak in $-\mathrm{Im}\{\chi^{(1)}\}$ [see Fig. 2(c)], and it constitutes the lowest energy excitation accessible within our driving protocol [82].

Formally, our analysis focuses on the two-point correlators, which we define in terms of the Fourier-transformed fields φ_k and Π_k:

$$\begin{aligned} \mathcal{D}_k^{\varphi}(t) &= \langle \varphi_{-k}(t)\varphi_k(t)\rangle, \\ \mathcal{D}_k^{\Pi}(t) &= \langle \Pi_{-k}(t)\Pi_k(t)\rangle, \\ \mathcal{D}_k^{X}(t) &= \frac{\langle\{\Pi_{-k}(t),\varphi_k(t)\}\rangle + \langle\{\varphi_{-k}(t),\Pi_k(t)\}\rangle}{2}. \end{aligned} \quad (3)$$

Note that since the SG Hamiltonian is translationally invariant, and the external drive is spatially homogeneous, Eq. (3) covers the entire set of nonzero two-point correlators. In the following, we analyze the second-order response of the system to the external perturbation described in Eq. (2), using a scheme similar to that of Ref. [30]. Specifically, a perturbative expansion of $\mathcal{D}_k^{\alpha}(\alpha = \varphi, \Pi, X)$ in powers of $\delta\Delta_0$ is performed up to second-order

$$\mathcal{D}_k^{\alpha}(t) = \mathcal{D}_{k,0}^{\alpha} + \mathcal{D}_{k,1}^{\alpha}(t) + \mathcal{D}_{k,2}^{\alpha}(t) + \ldots, \quad (4)$$

where the subindex i in $\mathcal{D}_{k,i}^{\alpha}$ represents the order in $\delta\Delta_0$, and $i = 0$ corresponds to the equilibrium thermal fluctuations. For completeness, a brief discussion of the system's linear response can be found in Ref. [55]. Before proceeding, we note that the equilibrium fluctuations computed within the Gaussian ansatz exhibit an ultraviolet divergence. Physically, this signals that the low-energy continuum theory should not be extrapolated to arbitrarily short distances, where a regularization is required. Since the fundamental bosons of the SG theory correspond to B_1 breathers [86], we implement this regularization by expressing the theory in terms of the physical mass M_{B_1} and drive $\delta\Delta$, rather than the bare couplings Δ_0 and $\delta\Delta_0$. Further details, including the computation of $\mathcal{D}_{k,0}^{\alpha}$, are provided in Ref. [55].

2D spectroscopy of fluctuation dynamics—In the 2DS framework, two perturbations $\delta\Delta_A$ and $\delta\Delta_B$ separated by a time delay $t_1 > 0$ are applied onto the system, see Fig. 1. At a time $t_2 > 0$ after the second perturbation, the momentum-resolved variance $\mathcal{D}_{k,AB}^{\varphi}$ is measured. A purely nonlinear response $\mathcal{D}_{k,\mathrm{nl}}^{\varphi}$ can be obtained by subtracting from $\mathcal{D}_{k,AB}^{\varphi}$ the contributions arising from single perturbations, such that

$$\mathcal{D}_{k,\mathrm{nl}}^{\varphi}(t_1,t_2) = \mathcal{D}_{k,AB}^{\varphi}(t_1,t_2) - \mathcal{D}_{k,A}^{\varphi}(t_1,t_2) - \mathcal{D}_{k,B}^{\varphi}(t_1,t_2), \quad (5)$$

where $\mathcal{D}_{k,A}^{\varphi}$ and $\mathcal{D}_{k,B}^{\varphi}$ are the measured variances when only perturbation $\delta\Delta_A$ and $\delta\Delta_B$ are present, respectively. Note that, for this system and protocol, we are probing the second-order response $\chi_k^{(2)}$, and that the nonlinear signal is directly proportional to $\delta\Delta_A\delta\Delta_B$. The nonlinear response, $\mathcal{D}_{k,\mathrm{nl}}^{\varphi}(t_1,t_2)$, is subsequently Fourier-transformed with respect to t_1 and t_2, under the constraint t_1, $t_2 > 0$. This results in $\mathcal{D}_{k,\mathrm{nl}}^{\varphi}(\omega_1,\omega_2)$, what we refer to as the 2D map, which is directly related to $\chi^{(2)}$ via

$$\begin{aligned} \mathcal{D}_{k,\mathrm{nl}}^{\varphi}(t_1,t_2) = 2\int \frac{d\omega_1}{2\pi}\int\frac{d\omega_2}{2\pi}\chi_k^{(2)}(\omega_1+\omega_2,\omega_1) \\ \times e^{-i\omega_1(t_1+t_2)}e^{-i\omega_2 t_2}\delta\Delta_A(\omega_1)\delta\Delta_B(\omega_2). \end{aligned} \quad (6)$$

We provide details of the calculation of $\chi^{(2)}$ within our Gaussian state ansatz, or by means of an equivalent diagrammatic approach, in Ref. [55].

Our protocol deviates from more common 2D approaches [26,30,54] in two main ways. First, the external perturbation couples to operators with even powers of the bosonic field, i.e., φ^{2n}, rather than to φ. This change has an important consequence: it produces a finite second-order response in powers of $\delta\Delta$, even when the system itself has no intrinsic nonlinearities. Second, the perturbation does not act on a single operator but instead couples to an infinite series of operators $\propto \cos(\beta\varphi)$, as shown in Eq. (2). This richer structure generates distinctive β-dependent features in the 2D map, which we illustrate in the following.

Before we proceed, it is helpful to note that, for small β, the pump-probe sector (corresponding to $\omega_1 = 0$) of the resulting maps is featureless, i.e., it shows no peaks. We have verified this by deriving the two-sided Feynman diagram rules for our protocol with a single bosonic excitation, see Supplemental Material [55]. Therefore, the discussion of the 2D spectra will focus on the nonrephasing and rephasing sectors, which correspond to the $\omega_1\omega_2 > 0$ and $\omega_1\omega_2 < 0$ quadrants of the 2D maps, respectively [87]. Note that the $\omega_1\omega_2$ sign indicates whether the two consecutive perturbations excite the system in phase (nonrephasing) or out of phase (rephasing).

We begin by considering the signatures in the nonrephasing sector of the 2D map ($\omega_1\omega_2 > 0$) as a function of β. Figures 3(a) and 3(b) show the same nonlinear response resolved by momentum, i.e., different fixed-k components of the 2D spectrum, for $\beta^2 = 2\pi$. Panel (a) corresponds to the $k = 0$ component. At this momentum, our choice of β is large enough for the B_2 binding energy to be appreciable, leading to two diagonal peaks: one at the $2B_1$ frequency associated with a pair of B_1 excitations, and one below the

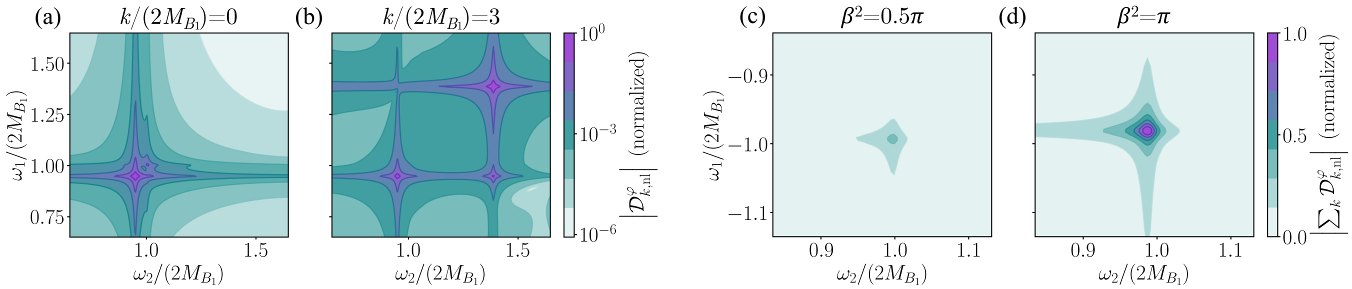

FIG. 3. (a), (b) The (normalized) k-resolved absolute value 2D map, $|\mathcal{D}^{\varphi}_{k,\mathrm{nl}}|$. Taking $\beta^2 = 2\pi$, we explore the system's nonrephasing sector for zero k [panel (a)] and for $k/(2M_{B_1}) = 3$ [panel (b)]. Panels (a) and (b) share the same logarithmic color scale. As k increases, the interplay between the B_1 continuum and the isolated B_2 becomes apparent, leading to asymmetric cross-peaks. This asymmetry is a hallmark of many-body dynamics absent in standard coupled-oscillator models. (c), (d) The (normalized) absolute value summed over k 2D map, $|\sum_k \mathcal{D}^{\varphi}_{k,\mathrm{nl}}|$. We focus on the system's rephasing sector for $\beta^2 = 0.5\pi$ [panel (c)] and $\beta^2 = \pi$ [panel (d)]. In both panels (c) and (d), the intensity is normalized to the $\beta^2 = \pi$ maximum (the color bar is shared). As β^2 increases, the system progressively becomes more interacting and the rephasing peak more prominent. In panels (a)–(d), frequencies are in units of the $2B_1$ mass, and a value $\eta = 0^+$ is chosen for the damping parameter.

two-particle continuum corresponding to the B_2 bound state. Panel (b) shows the same response at finite k. As the probed momentum increases, the characteristic peak spacings broaden overall, and off-diagonal features become visible. At first glance, our situation could seem analogous to the study of coupled molecules, where the 2D map provides information about their coupling strength, excitation pathways, and even Fermi resonances [87]. One could thus expect the characteristic four peak structure of coupled modes to manifest in our spectra. However, it is worth noting that the B_1 pairs constitute a continuum while the B_2 is a sharp, isolated excitation. The presence of this continuum leads to the suppression of one of the cross-peaks due to dephasing, resulting in the qualitatively distinct signature shown in Fig. 3(b), see Ref. [55] for more details and schematics. We emphasize that this striking many-body feature, arising from the interplay between an isolated mode and a continuum of excitations, is naturally revealed by the 2DS approach. Similar peak patterns have recently been reported in the context of magnetic systems [88].

We now turn to the rephasing sector ($\omega_1\omega_2 < 0$), whose name reflects its connection to the spin-echo phenomenon [89,90]. For $\beta \to 0$, it is devoid of any signatures: a distinctive feature of our protocol. Such behavior can be intuitively understood by approximating the external perturbation as $\cos(\beta\varphi) \sim \varphi^2$, and noting that no pathway can lead to echo-type processes at order $(\delta\Delta)^2$, see Supplemental Material for a detailed discussion [55]. This is, however, not the case for larger β, where the full cosine potential has to be considered. As such, the presence of the echo peak in the 2D spectra is a direct sign of a nonharmonicity of the system; equivalently, an indicator of the strength of interactions of the theory. We present the evolution of the echo peak as a function of β in Figs. 3(c) and 3(d), highlighting its progressive appearance as β increases [91].

Moreover, the echo peak is renowned for its ability to disentangle different sources of broadening. The paradigmatic example is in isolated two-level systems, where the echo peak can disentangle and quantify homogeneous and inhomogeneous broadening [92], a feature that lies beyond the reach of linear-response probes. Similar effects have been observed in exciton systems [51–53] and, more recently, in strongly correlated superconducting cuprates [26].

Of particular interest for the considered ultracold-atom system is the boson density, which determines β and Δ (as shown in the Appendix), thereby influencing the breather masses and the peak positions in the 2D map. Since observables in ultracold-atom experiments are typically obtained by averaging multiple destructive measurements, shot-to-shot fluctuations in the boson density, uncorrelated between distinct realizations, are expected. These fluctuations can affect the realization-averaged echo peak linewidths, in analogy to isolated two-level systems [92]. We investigate this aspect in Fig. 4, where we present the nonrephasing and rephasing (echo) peaks assuming a Gaussian distributed shot-to-shot density with mean $2\bar{M}_{B_1}$ and standard deviation $\sigma/(2\bar{M}_{B_1}) = 0.1$. The nonrephasing peak, see Fig. 4(a), symmetrically broadens with a shape indistinguishable from that of a damped mode. The echo peak instead presents a peculiar almond shape, see Fig. 4(b). Its extent along the $-\omega_1 = \omega_2$ diagonal roughly determines the shot-to-shot variance, while its broadening along $\omega_1 = \omega_2$ quantifies the intrinsic lifetime of the excitation. The distinct profiles of the nonrephasing and echo peaks motivate adopting NMR-inspired phenomenological fitting forms [92] to accurately determine damping and disorder in the ultracold atomic setup. Finally, we emphasize that performing such a disorder-versus-lifetime disentangling via linear response is very difficult in practice. This result clearly showcases the capabilities of 2DS over more traditional analysis methods.

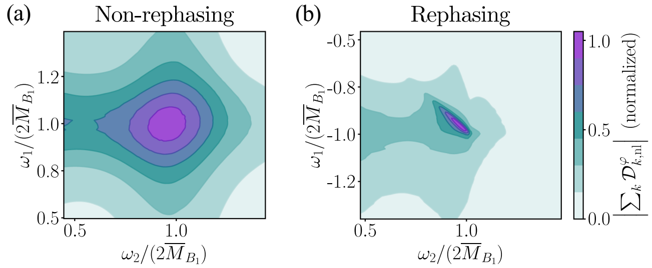

FIG. 4. The (normalized) summed over k absolute value 2D map, $|\sum_k \mathcal{D}^{\varphi}_{k,\mathrm{nl}}|$. Taking $\beta^2 = \pi$, we average over a shot-to-shot distribution assumed to be Gaussian for $2M_{B_1}$, with mean $2\bar{M}_{B_1}$ and standard deviation $\sigma/(2\bar{M}_{B_1}) = 0.1$. We focus on the system's nonrephasing [rephasing] sector in panel (a) [panel (b)]. Frequencies are normalized to the average $2B_1$ mass, a value $\eta = 0^+$ is chosen for the damping parameter, and the color bar is shared. On the one hand, the nonrephasing peak, see panel (a), becomes symmetrically broadened due to presence of shot-to-shot noise, with a shape indistinguishable from that of a damped mode. On the other hand, the almond-shaped rephasing peak in panel (b) provides a direct diagnostic of shot-to-shot density fluctuations, distinguishing them from intrinsic damping.

Conclusions and outlook—We investigated the nonlinear response of the SG model through a novel 2DS protocol. Our approach can be used to access the momentum-resolved nonlinear response functions, leveraging the spatial resolution of present-day ultracold atom platforms. The nonrephasing sector captures the interplay between continuum and discrete excitations, yielding asymmetric cross-peaks unique to the SG many-body dynamics. In contrast, the rephasing (echo) sector serves as a sensitive probe of interaction strength and of disorder, disentangling damping from shot-to-shot fluctuations.

The signatures predicted here can be directly tested with present atom-chip experiments on tunnel-coupled 1D Bose gases. Barrier modulation provides the required drive, while matter-wave interference gives access to momentum-resolved phase correlations. Typical system sizes, imaging resolution, and tunneling rates ensure that the relevant timescales lie well within condensate coherence times. Thus, the asymmetric cross-peaks and echolike disorder diagnostics we identify are experimentally accessible with current technology. Although a detailed implementation lies beyond the scope of this Letter, some practical considerations are outlined in the Appendix.

We note that our nonlinear spectroscopic analysis, presented at zero temperature, can be seamlessly adapted to incorporate finite-temperature effects by employing the self-consistent mean-field approximation. Furthermore, owing to the integrability of the SG model [82], our 2DS approach can be extended to account for the full nonlinear effects of the theory. To this end, the nonrephasing results from our protocol strongly indicate its suitability for studying matrix elements between breathers, building on the well-known form factors of the integrable theory $\sim\langle B_n|e^{i\beta\varphi}|0\rangle$ [82]. In this regard, we observe that the off-diagonal peak in Fig. 3(b) is proportional to well-known form factors and $\langle B_2(0)|\cos\beta\varphi|B_1(k)B_1(-k)\rangle$, while the diagonal ones correspond to $\langle B_2(0)|\cos\beta\varphi|B_2(0)\rangle$ and $\langle B_1(k)B_1(-k)|\cos\beta\varphi|B_1(k)B_1(-k)\rangle$ [93].

The combination of ultracold atomic systems and multidimensional spectroscopy opens the door to envisioning additional, more sophisticated protocols. For example, a scheme where the perturbation couples linearly to the field φ can go beyond the usual $k = 0$ coupling found in condensed matter platforms, enabling momentum-dependent coupling and resolution, and granting full access to the theory's T matrix.

Beyond the SG model, the same framework can be applied to other effective field theories realized in ultracold atoms (Lieb-Liniger gases, spin chains) and to engineered quantum devices (superconducting resonators, trapped ions). By accessing nonlinear matrix elements and form factors, momentum-resolved 2DS provides a route to directly test integrability, explore thermalization, and characterize exotic excitations in quantum simulators.

Acknowledgments—We thank D. Abanin, M. Aidelsburger, T. Andersen, I. Bloch, A. Carollo, R. Citro, V. Gritsev, F. Marijanovic, M. Michael, I. Morera, L. Skolc, B. Spagnolo, and A. Tsvelik for insightful discussions. A. G. S. and E. D. acknowledge the Swiss National Science Foundation (Grant No. 200021_212899) and ETH-C-06 21-2 equilibrium Grant with Project No. 1-008831-001 for funding. E. D. also acknowledges ARO Grant No. W911NF-20-1-0163. E. D. and D. V. acknowledge support from the CORI Project 2024 for the launch and development of international collaborations at the University of Palermo, which supported a scientific visit during which part of this work was carried out. D. D. S. acknowledges support from the Italian Ministry of University and Research (MUR), the "Angelo Della Riccia" Foundation, and ETH Zurich. N. B. and S. E. acknowledge support by the Austrian Science Fund (FWF) [Grant No. I6276, QuFT-Lab]. M. P. has received funding from Austrian Science Fund (FWF) [10.55776/ESP396; QuOntM]. J. S. has received funding from Austrian Science Fund (FWF) [Grant No. P36656, SCQS-oE].

Data availability—The data that support the findings of this article are openly available [94].

[1] D. C. Tsui, H. L. Stormer, and A. C. Gossard, Two-dimensional magnetotransport in the extreme quantum limit, Phys. Rev. Lett. **48**, 1559 (1982).

[2] R. B. Laughlin, Anomalous quantum Hall effect: An incompressible quantum fluid with fractionally charged excitations, Phys. Rev. Lett. **50**, 1395 (1983).

[3] F. D. M. Haldane, Effective harmonic-fluid approach to low-energy properties of one-dimensional quantum fluids, Phys. Rev. Lett. **47**, 1840 (1981).

[4] F. D. M. Haldane, 'Luttinger liquid theory' of one-dimensional quantum fluids. I. Properties of the Luttinger model and their extension to the general 1d interacting spinless Fermi gas, J. Phys. C **14**, 2585 (1981).

[5] T. Giamarchi, *Quantum Physics in One Dimension* (Clarendon Press, Oxford, 2003).

[6] I. Bloch, J. Dalibard, and W. Zwerger, Many-body physics with ultracold gases, Rev. Mod. Phys. **80**, 885 (2008).

[7] M. A. Cazalilla, R. Citro, T. Giamarchi, E. Orignac, and M. Rigol, One dimensional bosons: From condensed matter systems to ultracold gases, Rev. Mod. Phys. **83**, 1405 (2011).

[8] T. Langen, R. Geiger, and J. Schmiedmayer, Ultracold atoms out of equilibrium, Annu. Rev. Condens. Matter Phys. **6**, 201 (2015).

[9] C. Gross and I. Bloch, Quantum simulations with ultracold atoms in optical lattices, Science **357**, 995 (2017).

[10] C. Monroe, W. C. Campbell, L.-M. Duan, Z.-X. Gong, A. V. Gorshkov, P. W. Hess, R. Islam, K. Kim, N. M. Linke, G. Pagano *et al.*, Programmable quantum simulations of spin systems with trapped ions, Rev. Mod. Phys. **93**, 025001 (2021).

[11] A. D. King, S. Suzuki, J. Raymond, A. Zucca, T. Lanting, F. Altomare, A. J. Berkley, S. Ejtemaee, E. Hoskinson, S. Huang *et al.*, Coherent quantum annealing in a programmable 2,000 qubit Ising chain, Nat. Phys. **18**, 1324 (2022).

[12] A. Guinier, *X-Ray Diffraction in Crystals, Imperfect Crystals, and Amorphous Bodies* (Dover Publications, New York, 1994).

[13] R. Comin and A. Damascelli, Resonant x-ray scattering studies of charge order in cuprates, Annu. Rev. Condens. Matter Phys. **7**, 369 (2016).

[14] J. Jimenez and J. W. Tomm, Basics of optical spectroscopy: Transmission and reflection measurements, their analysis, and related techniques, in *Spectroscopic Analysis of Optoelectronic Semiconductors* (Springer International Publishing, Cham, 2016), pp. 49–76.

[15] R. Robson, R. White, and M. Hildebrandt, *Fundamentals of Charged Particle Transport in Gases and Condensed Matter* (CRC Press, Boca Raton, 2017).

[16] J. P. Pekola and B. Karimi, Colloquium: Quantum heat transport in condensed matter systems, Rev. Mod. Phys. **93**, 041001 (2021).

[17] S. Gupta, Z. Hadzibabic, M. W. Zwierlein, C. A. Stan, K. Dieckmann, C. H. Schunck, E. G. M. van Kempen, B. J. Verhaar, and W. Ketterle, Radio-frequency spectroscopy of ultracold fermions, Science **300**, 1723 (2003).

[18] M. Endres, T. Fukuhara, D. Pekker, M. Cheneau, and P. Schauß, C. Gross, E. Demler, S. Kuhr, and I. Bloch, The 'Higgs' amplitude mode at the two-dimensional superfluid/mott insulator transition, Nature (London) **487**, 454 (2012).

[19] M. L. Prichard, Z. Ba, I. Morera, B. M. Spar, D. A. Huse, E. Demler, and W. S. Bakr, Magnon-polarons in the Fermi–Hubbard model, Nat. Phys. **21**, 1548 (2025).

[20] A. Autere, H. Jussila, A. Marini, J. R. M. Saavedra, Y. Dai, A. Säynätjoki, L. Karvonen, H. Yang, B. Amirsolaimani, R. A. Norwood, N. Peyghambarian, H. Lipsanen, K. Kieu, F. J. G. de Abajo, and Z. Sun, Optical harmonic generation in monolayer group-VI transition metal dichalcogenides, Phys. Rev. B **98**, 115426 (2018).

[21] G. Seibold, M. Udina, C. Castellani, and L. Benfatto, Third harmonic generation from collective modes in disordered superconductors, Phys. Rev. B **103**, 014512 (2021).

[22] M.-J. Kim, S. Kovalev, M. Udina, R. Haenel, G. Kim, M. Puviani, G. Cristiani, I. Ilyakov, T. V. A. G. de Oliveira, A. Ponomaryov, J.-C. Deinert, G. Logvenov, B. Keimer, D. Manske, L. Benfatto, and S. Kaiser, Tracing the dynamics of superconducting order via transient terahertz third-harmonic generation, Sci. Adv. **10**, eadi7598 (2024).

[23] A. Liu, Multidimensional terahertz probes of quantum materials, npj Quantum Mater. **10**, 18 (2025).

[24] C. Huang, M. Mootz, L. Luo, I. E. Perakis, and J. Wang, Unlocking quantum control and multi-order correlations via terahertz two-dimensional coherent spectroscopy, arXiv:2507.02116.

[25] M. Mootz, L. Luo, J. Wang, and I. E. Perakis, Visualization and quantum control of light-accelerated condensates by terahertz multi-dimensional coherent spectroscopy, Commun. Phys. **5**, 47 (2022).

[26] A. Liu, D. Pavićević, M. H. Michael, A. G. Salvador, P. E. Dolgirev, M. Fechner, A. S. Disa, P. M. Lozano, Q. Li, G. D. Gu, E. Demler, and A. Cavalleri, Probing inhomogeneous cuprate superconductivity by terahertz Josephson echo spectroscopy, Nat. Phys. **20**, 1751 (2024).

[27] K. Katsumi, J. Fiore, M. Udina, R. Romero, D. Barbalas, J. Jesudasan, P. Raychaudhuri, G. Seibold, L. Benfatto, and N. P. Armitage, Revealing novel aspects of light-matter coupling by terahertz two-dimensional coherent spectroscopy: The case of the amplitude mode in superconductors, Phys. Rev. Lett. **132**, 256903 (2024).

[28] M. Puviani, Theory of symmetry-resolved quench-drive spectroscopy: Nonlinear response of phase-fluctuating superconductors, Phys. Rev. B **109**, 214515 (2024).

[29] K. Katsumi, J. Liang, R. R. III, K. Chen, X. Xi, and N. P. Armitage, Amplitude mode in a multigap superconductor MgB_2 investigated by terahertz two-dimensional coherent spectroscopy, Phys. Rev. Lett. **135**, 036902 (2025).

[30] A. Gómez Salvador, P. E. Dolgirev, M. H. Michael, A. Liu, D. Pavicevic, M. Fechner, A. Cavalleri, and E. Demler, Principles of two-dimensional terahertz spectroscopy of collective excitations: The case of Josephson plasmons in layered superconductors, Phys. Rev. B **110**, 094514 (2024).

[31] D. Barbalas, R. Romero III, D. Chaudhuri, F. Mahmood, H. P. Nair, N. J. Schreiber, D. G. Schlom, K. Shen, and N. Armitage, Energy relaxation and dynamics in the correlated metal Sr_2 RuO_4 via THz two-dimensional coherent spectroscopy, arXiv:2312.13502.

[32] J. Chen and P. Werner, Multidimensional coherent spectroscopy of correlated lattice systems, npj Comput Mater. **11**, 127 (2025).

[33] J. Lu, X. Li, H. Y. Hwang, B. K. Ofori-Okai, T. Kurihara, T. Suemoto, and K. A. Nelson, Coherent two-dimensional terahertz magnetic resonance spectroscopy of collective spin waves, Phys. Rev. Lett. **118**, 207204 (2017).

[34] H.-W. Lin, G. Mead, and G. A. Blake, Mapping $LiNbO_3$ phonon-polariton nonlinearities with 2d THz-THz-Raman spectroscopy, Phys. Rev. Lett. **129**, 207401 (2022).

[35] Z. Zhang, F. Y. Gao, Y.-C. Chien, Z.-J. Liu, J. B. Curtis, E. R. Sung, X. Ma, W. Ren, S. Cao, P. Narang, A. von Hoegen, E. Baldini, and K. A. Nelson, Terahertz-field-driven magnon upconversion in an antiferromagnet, Nat. Phys. **20**, 788 (2024).

[36] Z. Zhang, F. Y. Gao, J. B. Curtis, Z.-J. Liu, Y.-C. Chien, A. von Hoegen, M. T. Wong, T. Kurihara, T. Suemoto, P. Narang, E. Baldini, and K. A. Nelson, Terahertz field-induced nonlinear coupling of two magnon modes in an antiferromagnet, Nat. Phys. **20**, 801 (2024).

[37] S. A. Parameswaran and S. Gopalakrishnan, Asymptotically exact theory for nonlinear spectroscopy of random quantum magnets, Phys. Rev. Lett. **125**, 237601 (2020).

[38] T. G. H. Blank, K. A. Grishunin, K. A. Zvezdin, N. T. Hai, J. C. Wu, S.-H. Su, J.-C. A. Huang, A. K. Zvezdin, and A. V. Kimel, Two-dimensional terahertz spectroscopy of nonlinear phononics in the topological insulator $MnBi_2Te_4$, Phys. Rev. Lett. **131**, 026902 (2023).

[39] Y. Wan and N. P. Armitage, Resolving continua of fractional excitations by spinon echo in THz 2D coherent spectroscopy, Phys. Rev. Lett. **122**, 257401 (2019).

[40] O. Liebman, J. Curtis, I. Petrides, and P. Narang, Multiphoton spectroscopy of a dynamical axion insulator, Phys. Rev. Lett. **135**, 196601 (2025).

[41] W. Choi, K. H. Lee, and Y. B. Kim, Theory of two-dimensional nonlinear spectroscopy for the Kitaev spin liquid, Phys. Rev. Lett. **124**, 117205 (2020).

[42] M. McGinley, M. Fava, and S. A. Parameswaran, Signatures of fractional statistics in nonlinear pump-probe spectroscopy, Phys. Rev. Lett. **132**, 066702 (2024).

[43] M. McGinley, M. Fava, and S. A. Parameswaran, Anomalous thermal relaxation and pump-probe spectroscopy of two-dimensional topologically ordered systems, Phys. Rev. B **109**, 075108 (2024).

[44] M. Potts, R. Moessner, and O. Benton, Signatures of spinon dynamics and phase structure of dipolar-octupolar quantum spin ices in two-dimensional coherent spectroscopy, Phys. Rev. Lett. **133**, 226701 (2024).

[45] B. Lomsadze and S. T. Cundiff, Frequency combs enable rapid and high-resolution multidimensional coherent spectroscopy, Science **357**, 1389 (2017).

[46] A. Liu, D. B. Almeida, W. K. Bae, L. A. Padilha, and S. T. Cundiff, Non-markovian exciton-phonon interactions in core-shell colloidal quantum dots at femtosecond timescales, Phys. Rev. Lett. **123**, 057403 (2019).

[47] J. B. Muir, J. Levinsen, S. K. Earl, M. A. Conway, J. H. Cole, M. Wurdack, R. Mishra, D. J. Ing, E. Estrecho, Y. Lu, D. K. Efimkin, J. O. Tollerud, E. A. Ostrovskaya, M. M. Parish, and J. A. Davis, Interactions between Fermi polarons in monolayer WS_2, Nat. Commun. **13**, 6164 (2022).

[48] K. W. Stone, K. Gundogdu, D. B. Turner, X. Li, S. T. Cundiff, and K. A. Nelson, Two-quantum 2D FT electronic spectroscopy of biexcitons in gaas quantum wells, Science **324**, 1169 (2009).

[49] K. Hao, L. Xu, F. Wu, P. Nagler, K. Tran, X. Ma, C. Schüller, T. Korn, A. H. MacDonald, G. Moody *et al.*, Trion valley coherence in monolayer semiconductors, 2D Mater. **4**, 025105 (2017).

[50] K. Hao, J. F. Specht, P. Nagler, L. Xu, K. Tran, A. Singh, C. K. Dass, C. Schüller, T. Korn, M. Richter, A. Knorr, X. Li, and G. Moody, Neutral and charged inter-valley biexcitons in monolayer $MoSe_2$, Nat. Commun. **8**, 15552 (2017).

[51] A. Bristow, T. Zhang, M. Siemens, S. Cundiff, and R. Mirin, Separating homogeneous and inhomogeneous line widths of heavy- and light-hole excitons in weakly disordered semiconductor quantum wells, J. Phys. Chem. B **115**, 5365 (2011).

[52] G. Moody, C. Kavir Dass, K. Hao, C.-H. Chen, L.-J. Li, A. Singh, K. Tran, G. Clark, X. Xu, G. Berghäuser, E. Malic, A. Knorr, and X. Li, Intrinsic homogeneous linewidth and broadening mechanisms of excitons in monolayer transition metal dichalcogenides, Nat. Commun. **6**, 8315 (2015).

[53] D. Huang, K. Sampson, Y. Ni, Z. Liu, D. Liang, K. Watanabe, T. Taniguchi, H. Li, E. Martin, J. Levinsen, M. M. Parish, E. Tutuc, D. K. Efimkin, and X. Li, Quantum dynamics of attractive and repulsive polarons in a doped $MoSe_2$ monolayer, Phys. Rev. X **13**, 011029 (2023).

[54] A. G. Salvador, I. Morera, M. H. Michael, P. E. Dolgirev, D. Pavicevic, A. Liu, A. Cavalleri, and E. Demler, Two-dimensional spectroscopy of bosonic collective excitations in disordered many-body systems, arXiv:2501.16856.

[55] See Supplemental Material at http://link.aps.org/supplemental/10.1103/tfdm-qshs for additional information on the equations of motion, equilibrium and dynamical correlators, linear response, two-sided Feynman diagrams for a single bosonic excitation, the asymmetry of the rephasing signature, and a diagrammatic understanding of the Gaussian-state ansatz. Supplemental Material includes Refs. [56–59].

[56] T. Shi, E. Demler, and J. Ignacio Cirac, Variational study of fermionic and bosonic systems with non-Gaussian states: Theory and applications, Ann. Phys. (Amsterdam) **390**, 245 (2018).

[57] K. Maki and H. Takayama, Breathers in the sine-Gordon system at finite temperatures, Phys. Rev. B **22**, 5302 (1980).

[58] A. B. Zamolodchikov, Mass scale in the sine–Gordon model and its reductions, Int. J. Mod. Phys. A **10**, 1125 (1995).

[59] S. Mukamel, *Principles of Nonlinear Optical Spectroscopy*, Oxford Series in Optical and Imaging Sciences (Oxford University Press, New York, 1995).

[60] T. Dauxois and M. Peyrard, *Physics of Solitons* (Cambridge University Press, Cambridge, England, 2006).

[61] A. Torrielli, *Integrability using the Sine-Gordon and Thirring Duality* (IOP Publishing, 2024), pp. 2053–2563, 10.1088/978-0-7503-5899-6.

[62] S. Coleman, Quantum sine-Gordon equation as the massive Thirring model, Phys. Rev. D **11**, 2088 (1975).

[63] L. Benfatto, C. Castellani, and T. Giamarchi, Sine-Gordon description of Beresinskii-Kosterlitz-Thouless vortices in superconductors immersed in an external magnetic field, Phys. Rev. Lett. **99**, 207002 (2007).

[64] R. Citro, E. G. Dalla Torre, L. D'Alessio, A. Polkovnikov, M. Babadi, T. Oka, and E. Demler, Dynamical stability of a many-body Kapitza pendulum, Ann. Phys. (N.Y.) **360**, 694 (2015).

[65] T. Schweigler, V. Kasper, S. Erne, I. Mazets, B. Rauer, F. Cataldini, T. Langen, T. Gasenzer, J. Berges, and J. Schmiedmayer, Experimental characterization of a quantum many-body system via higher-order correlations, Nature (London) **545**, 323 (2017).

[66] R. Citro, E. Demler, T. Giamarchi, M. Knap, and E. Orignac, Lattice modulation spectroscopy of one-dimensional quantum gases: Universal scaling of the absorbed energy, Phys. Rev. Res. **2**, 033187 (2020).

[67] T. Schweigler, M. Gluza, M. Tajik, S. Sotiriadis, F. Cataldini, S.-C. Ji, F. S. Møller, J. Sabino, B. Rauer, J. Eisert *et al.*, Decay and recurrence of non-Gaussian correlations in a quantum many-body system, Nat. Phys. **17**, 559 (2021).

[68] I. Lovas, R. Citro, E. Demler, T. Giamarchi, M. Knap, and E. Orignac, Many-body parametric resonances in the driven sine-Gordon model, Phys. Rev. B **106**, 075426 (2022).

[69] J. Cuevas-Maraver, P. G. Kevrekidis, and F. Williams, *The Sine-Gordon Model and its Applications* (Springer, New York, 2014).

[70] M. H. Michael, D. De Santis, E. A. Demler, and P. A. Lee, Giant dynamical paramagnetism in the driven pseudogap phase of $YBa_2Cu_3O_{6+x}$, arXiv:2410.12919.

[71] D. De Santis, D. Valenti, B. Spagnolo, G. Di Fresco, A. Carollo, and C. Guarcello, Noisy sine-Gordon breather dynamics: A short review, Chaos Solitons Fractals **199**, 116641 (2025).

[72] P. Lee, T. Rice, and P. Anderson, Conductivity from charge or spin density waves, Solid State Commun. **14**, 703 (1974).

[73] M. J. Rice, A. R. Bishop, J. A. Krumhansl, and S. E. Trullinger, Weakly pinned Fröhlich charge-density-wave condensates: A new, nonlinear, current-carrying elementary excitation, Phys. Rev. Lett. **36**, 432 (1976).

[74] T. Asano, H. Nojiri, Y. Inagaki, J. Boucher, T. Sakon, Y. Ajiro, and M. Motokawa, Esr investigation on the breather mode and the spinon-breather dynamical crossover in Cu benzoate, Phys. Rev. Lett. **84**, 5880 (2000).

[75] A. C. Tiegel, A. Honecker, T. Pruschke, A. Ponomaryov, S. A. Zvyagin, R. Feyerherm, and S. R. Manmana, Dynamical properties of the sine-Gordon quantum spin magnet Cu-Pm at zero and finite temperature, Phys. Rev. B **93**, 104411 (2016).

[76] A. M. Visuri, M. Lebrat, S. Häusler, L. Corman, and T. Giamarchi, Spin transport in a one-dimensional quantum wire, Phys. Rev. Res. **2**, 023062 (2020).

[77] E. Wybo, M. Knap, and A. Bastianello, Quantum sine-Gordon dynamics in coupled spin chains, Phys. Rev. B **106**, 075102 (2022).

[78] E. Wybo, A. Bastianello, M. Aidelsburger, I. Bloch, and M. Knap, Preparing and analyzing solitons in the sine-Gordon model with quantum gas microscopes, PRX Quantum **4**, 030308 (2023).

[79] S. M. Girvin and A. H. MacDonald, Multi-component quantum Hall systems: The sum of their parts and more, arXiv:cond-mat/9505087.

[80] V. Zharnitsky, I. Mitkov, and M. Levi, Parametrically forced sine-Gordon equation and domain wall dynamics in ferromagnets, Phys. Rev. B **57**, 5033 (1998).

[81] T. I. Andersen *et al.*, Thermalization and criticality on an analogue–digital quantum simulator, Nature (London) **638**, 79 (2024).

[82] V. Gritsev, A. Polkovnikov, and E. Demler, Linear response theory for a pair of coupled one-dimensional condensates of interacting atoms, Phys. Rev. B **75**, 174511 (2007).

[83] M. Malard, Sine-Gordon model: Renormalization group solution and applications, Braz. J. Phys. **43**, 182 (2013).

[84] Within this regime, the specific β^2 values used in our figures are chosen primarily for visualization purposes. As for the tunnel coupling, we present below results normalized by this quantity.

[85] A generalization to spatially dependent scenarios [82] is straightforward. We also note that while our subsequent results are derived for a generic $\delta\Delta_0(t)$, for plotting purposes we mostly focus on impulsive (delta-like) forcing profiles.

[86] V. Gritsev, E. Demler, M. Lukin, and A. Polkovnikov, Spectroscopy of collective excitations in interacting low-dimensional many-body systems using quench dynamics, Phys. Rev. Lett. **99**, 200404 (2007).

[87] P. Hamm and M. Zanni, *Concepts and Methods of 2D Infrared Spectroscopy* (Cambridge University Press, Cambridge, England, 2011), 10.1017/CBO9780511675935.

[88] Y. Watanabe, S. Trebst, and C. Hickey, Revealing quadrupolar excitations with nonlinear spectroscopy, Phys. Rev. Lett. **134**, 106703 (2025).

[89] E. L. Hahn, Spin echoes, Phys. Rev. **80**, 580 (1950).

[90] M. Cetina, M. Jag, R. S. Lous, J. T. M. Walraven, R. Grimm, R. S. Christensen, and G. M. Bruun, Decoherence of impurities in a Fermi sea of ultracold atoms, Phys. Rev. Lett. **115**, 135302 (2015).

[91] We note that Figs. 3(c) and 3(d) presents the system's response summed over all k, where the bound state is expected to dominate (as indicated by the linear response). This accounts for the appearance of only a sub-$2B_1$ peak in this case. Rephasing phenomena are observed, in a similar fashion, in the k-resolved case as well.

[92] M. E. Siemens, G. Moody, H. Li, A. D. Bristow, and S. T. Cundiff, Resonance lineshapes in two-dimensional fourier transform spectroscopy, Opt. Express **18**, 17699 (2010).

[93] Note that in Fig. 3 we plot the absolute-value peak, but both real and imaginary parts are in principle experimentally accessible, enabling their full characterization.

[94] D. De Santis, A. Gómez-Salvador, and E. Demler, Zenodo, duilio-desantis/2ds-sg: 2ds-sg (2026), 10.5281/zenodo.20021658.

[95] Z. Wang, H. Da, A. S. Disa, T. Pullerits, A. Liu, and F. Schlawin, Sparse optimization of two-dimensional terahertz spectroscopy, APL Photonics **10**, 096107 (2025).

End Matter

Appendix: Coupled 1D condensates as a SG experimental realization—A prototypal experimental realization of the quantum SG model, first proposed in Ref. [82], consists of two tunnel-coupled (quasi) 1D condensates. Following Refs. [65,67], we consider a system of ultracold bosons (Rubidium-87 atoms) trapped in a double-well potential on an atom chip. The double-well potential, engineered via rf magnetic fields, features a barrier that can be tuned by adjusting such fields' amplitude. In other words, the tunneling rate between the condensates is a highly controllable quantity, a fact which motivates our choice for the driving protocol made in this work. Then, matter-wave interference grants access to the spatially resolved phase difference between the superfluids. This phase difference can be Fourier-transformed into momentum space and averaged over multiple experimental runs. The resulting data under a single perturbation (or two consecutive time-delayed perturbations) provide direct experimental counterparts to the 1D spectra (or 2D maps) discussed in our work. See below for further details.

In typical experimental setups [65,67], both wells are confined tightly (weakly) in the radial (longitudinal) direction, such that the system is effectively one dimensional. In this regime, the radial dynamics is frozen, while the double-well barrier still allows for tunneling between the two condensates. After integrating out the radial degrees of freedom, one obtains the following 1D effective Hamiltonian:

$$H=\sum_{j=1}^{2}\int dx\left\{\frac{\hbar^2}{2m}\partial_x\psi_j^\dagger\partial_x\psi_j+\frac{g_{1D}}{2}\psi_j^\dagger\psi_j^\dagger\psi_j\psi_j + [U(x)-\mu]\psi_j^\dagger\psi_j\right\}-\hbar J\int dx\left[\psi_1^\dagger\psi_2+\psi_2^\dagger\psi_1\right], \qquad (A1)$$

where the field operators fulfill bosonic commutation relations, $[\psi_j(x),\psi_{j'}^\dagger(x')]=\delta_{jj'}\,\delta(x-x')$, m is the atomic mass, g_{1D} the effective 1D interaction strength, $U(x)$ the longitudinal trapping potential (set to zero in the following for simplicity), and J the tunneling rate.

The effective coupling g_{1D} can be written in terms of the s-wave scattering length a_s and the 1D density n_{1D} as

$$g_{1D}=\hbar\omega_\perp a_s\frac{2+3a_sn_{1D}}{1+2a_sn_{1D}}. \qquad (A2)$$

Working in the density-phase representation,

$$\psi_j(x)=e^{i\theta_j(x)}\sqrt{n_{1D}+\delta n_j(x)}, \qquad (A3)$$

we introduce the relative degrees of freedom

$$\varphi(x)=\theta_1(x)-\theta_2(x),\quad \rho(x)=\frac{1}{2}[\delta n_1(x)-\delta n_2(x)], \qquad (A4)$$

which satisfy canonical commutation relations. Expanding the Hamiltonian to second order in $\partial_x\varphi$ and ρ, one finds

$$H=\int dx\left[\frac{\hbar^2 n_{1D}}{4m}(\partial_x\varphi)^2+\frac{\hbar^2}{4mn_{1D}}(\partial_x\rho)^2 + g\rho^2-2\hbar Jn_{1D}\cos\varphi\right], \qquad (A5)$$

with $g=g_{1D}+\hbar J/n_{1D}$. Since density fluctuations are strongly suppressed in the low-energy regime of interest, the density gradient term may be neglected, yielding the SG Hamiltonian

$$H=\int dx\left[\frac{\hbar^2 n_{1D}}{4m}(\partial_x\varphi)^2+g\rho^2-2\hbar Jn_{1D}\cos\varphi\right]. \qquad (A6)$$

For $J=0$ this reduces to the Luttinger Hamiltonian. Introducing the rescaled fields $\varphi\to\varphi/\beta$ and $\Pi=\beta\rho$, with $\beta^2=2\pi/K$ and K the Luttinger parameter, the Hamiltonian becomes

$$H=\frac{\hbar c_s}{2}\int dx\left[(\partial_x\varphi)^2+\Pi^2-\frac{4Jn_{1D}}{c_s}\cos(\beta\varphi)\right], \qquad (A7)$$

where $c_s=\sqrt{gn_{1D}/m}$ is the sound velocity. Finally, introducing a reference length scale x_0, one can write

$$H=\frac{\hbar c_s}{2x_0}\int dx\left[(\partial_x\varphi)^2+\Pi^2-\Delta\cos(\beta\varphi)\right], \qquad (A8)$$

with the dimensionless parameter $\Delta=8Jmx_0^2/(\beta^2\hbar)$.

Typical experimental parameters—In cold-atom realizations with ^{87}Rb [65,67], typical values are radial trapping frequencies of order $\omega_\perp/2\pi\sim$ kHz and longitudinal frequencies of order $\omega_x/2\pi\sim$ few Hz; interaction energies $\mu/\hbar$ and thermal energies $k_BT/\hbar$ in the few hundred Hz range, both below $\omega_\perp$, ensuring effective one-dimensionality; s-wave scattering length $a_s\approx 5$ nm; mean 1D densities $n_{1D}\sim 10$–$100\ \mu\mathrm{m}^{-1}$; and tunneling rates J ranging from a few to a few tens of Hz. Regarding the momentum range accessible within the coupled-condensates realization, a reasonable upper bound for k can be estimated from the spatial resolution of the phase measurement, which is in turn limited by the pixel size Δx_{pix}, on the order of $\Delta x_{\mathrm{pix}}\sim 2\ \mu\mathrm{m}$ [67]. We therefore have $k_{\max}\sim 2\pi/\Delta x_{\mathrm{pix}}\sim 3\ \mu\mathrm{m}^{-1}$. The lower bound for k is set by the length L of the cigar-shaped atomic clouds illustrated in Fig. 2(a) of the Letter, typically $L\sim 50\,\mu\mathrm{m}$. We thus estimate $k_{\min}\sim 2\pi/L\sim 0.1\ \mu\mathrm{m}^{-1}$. These values illustrate that the assumptions made in the derivation of the effective SG description are well justified in typical experiments.

Practical implementation and measurements—In tunnel-coupled 1D Bose gases on atom chips (see Refs. [65,67]), the modulation $\delta\Delta(t)$ used in our theory corresponds to a controlled change of the barrier height.

In practice, this is achieved by tuning the amplitude of the radio frequency or optical fields that generate the double-well potential. Such modulations on millisecond timescales are standard and have already been demonstrated experimentally. Regarding the strength of the perturbation, consisting of either a periodic or impulsive modulation of the tunneling rate J between the condensates, it must be kept weak enough for (i) our perturbative treatment to remain valid, yet sufficiently strong for (ii) the resulting nonlinearities to be experimentally measurable. In practice, these two conditions can be checked by (i) examining the scaling of the nonlinear response with the perturbation strength and (ii) ensuring that an appreciable signal remains after subtraction (discussed in the main text) of the linear-response signal.

The relevant observables are directly accessible: matter-wave interference yields the spatially resolved relative phase $\varphi(x)$ between the condensates. Fourier transforming these phase profiles provides the momentum-resolved correlators $\mathcal{D}_k^{\varphi}$, which are averaged over multiple runs. These measured quantities correspond one-to-one with the theoretical spectra and 2D maps presented in the main text.

Experimentally, typical system sizes (about 100 micrometers) and imaging resolutions (a few micrometers) give access to the required momentum range. The characteristic timescales of the protocol, determined by the tunneling rate J (a few Hz to tens of Hz), remain well within condensate coherence times. Shot-to-shot fluctuations in atom number translate into variations of $\mathcal{D}_k^{\varphi}$, naturally reproducing the type of inhomogeneous broadening discussed in Fig. 4 of the main text. We estimate that a few hundred to a thousand realizations are sufficient to reconstruct the 2D maps with adequate signal-to-noise, in line with current practice in phase-correlation measurements. The estimate for the number of realizations is based on earlier experimental studies of nonequilibrium dynamics performed on the coupled-condensate platform [65,67], in which time-resolved higher-order phase correlators were efficiently sampled over 100–1000 independent experimental runs.

Finally, it may be worth commenting on the time-consuming nature of the 2DS approach. We first note that this can be mitigated by focusing on the most informative sectors of the map, using simpler one-dimensional scans to precharacterize the resonance frequencies. Furthermore, we emphasize that this challenge is not specific to the cold-atom implementation. In fact, it has also been recognized as a key issue in 2DS in the optical, infrared, and, more recently, terahertz regimes, and substantial efforts have been devoted to accelerating the technique. A recent example from the THz 2DS community can be found in Wang *et al.* [95], where signal reconstruction via compressive sensing is used to show that long experimental acquisition times can be substantially reduced. We believe that, as the field of nonlinear spectroscopy in cold atoms matures, this and related works may pave the way for similar acceleration strategies in cold-atom implementations of 2DS.